Measurement of mass transport and reaction parameters in bulk solution using photobleaching

Reaction limited binding regime

Eric Neil Kaufman and Rakesh K. Jain
Department of Chemical Engineering, Carnegie Mellon University, Pittsburgh, Pennsylvania, 15213-3890 USA

ABSTRACT Fluorescence recovery after photobleaching (FRAP) has been used previously to investigate the kinetics of binding to biological surfaces. The present study adapts and further develops this technique for the quantification of mass transport and reaction parameters in bulk media. The technique's ability to obtain the bulk diffusion coefficient, concentration of binding sites, and equilibrium binding constant for ligand/receptor interactions in the reaction limited binding regime is assessed using the B72.3/TAG-72 monoclonal antibody/tumor associated antigen interaction as a model in vitro system. Measurements were independently verified using fluorometry. The bulk diffusion coefficient, concentration of binding sites and equilibrium binding constant for the system investigated were $6.1 \pm 1.1 \times 10^{-7}$ cm^2/s, $4.4 \pm 0.6 \times 10^{-7}$ M, and $2.5 \pm 1.6 \times 10^{7}$ M^{-1}, respectively. Model robustness and the applicability of the technique for in vivo quantification of mass transport and reaction parameters are addressed. With a suitable animal model, it is believed that this technique is capable of quantifying mass transport and reaction parameters in vivo.

INTRODUCTION

Mass transport and reaction govern the distribution of a species in porous media in a wide range of applications including oil recovery, chemical reactor design, and cancer research. Recent theoretical (1–6) and experimental (7–10) work has investigated the importance of transport and reaction parameters in the distribution of therapeutic agents to diseased tissue in the human body. In particular, it has been proposed that the various resistances to mass transport encountered by monoclonal antibodies may account for their poor distribution and limited success in detecting and treating cancer (11). Whereas the theoretical significance of these parameters has been established, there exist few experimental techniques capable of in vivo quantification. No technique currently exists capable of accurately and noninvasively quantifying the diffusion coefficient and binding parameters characterizing a therapeutic agent's distribution in the interstitial space of a tissue. This paper discusses the development and validation of a photobleaching technique for the determination of the diffusion coefficient, equilibrium binding constant, and binding site concentration for a reaction limited binding system. Whereas experimentation in this paper is carried out in vitro, the method is general, and is amenable to in vivo use.

There have been many in vitro measurements of affinity binding constants and concentration of binding sites for monoclonal antibody/tumor associated antigen systems. A sampling of the systems investigated, experimental methods used, and their results is shown in Table 1. Most studies have used a solid phase immunoassay technique coupled with variations of Scatchard analysis (12). In an attempt to develop a system more representative of the in vivo environment, binding rates, and diffusion coefficients have been quantified by measuring the rate of uptake and subsequent washout of radiolabeled antibodies from tumor spheroids (13). Whereas in vitro methods have proven valuable in screening monoclonal antibodies and assessing their relative reactivities, questions arise as to their usefulness in predicting in vivo drug distribution due to differences between in vivo and in vitro antigen expression (14–16) and mode of binding (Kaufman, E. N., and R. K. Jain, in preparation). In vivo data of drug concentration in plasma and tissue as a function of time post injection has been fit to two compartment pharmacokinetic models in order to quantify the product of the equilibrium binding constant and the concentration of binding sites (17). Such studies model the tissue as a well mixed reactor volume. This assumption poses an apparent contradiction. By assuming the tissue as well mixed, the system is modeled as being reaction limited. However, the models fit the data to obtain the diffusion limited kinetic parameter (18). Possible parameter error as a result of this discrepancy is currently under investigation (Kaufman, E. N., and R. K. Jain, in preparation).

It is seen that there is a need for a noninvasive, in vivo

Please address reprint requests to Dr. Jain at A. W. Cook Professor of Tumor Biology, Harvard Medical School and Director, E. L. Steele Lab, Massachusetts General Hospital, Boston MA 02114.

0006-3495/91/09/596/15 $2.00

TABLE 1 **Sampling of results obtained from various in vitro binding assays**

System	Method	Results		Reference
IgG anti Thy 1.1 antibody 31E6.4/AKR15 SL2 murine lymphoma cells	cell binding assay (12)	$K_{eq} = 3.5 \times 10^9\ M^{-1}$ 5×10^5 sites/cell		(39)
IgG LS2D617/human small cell lung carcinoma	cell binding assay (12)	$K_{eq} = 1 \times 10^8\ M^{-1}$ 2×10^6 sites/cell		(56)
IgG anti Thy 1.1 antibody 1A14/T cell differentiation antigen	cell binding assay (12)	$K_{eq} = 1.6 \times 10^9\ M^{-1}$		(57)
IgG antibodies/TAG-72 tumor associated antigen	solid phase immunoassay using purified TAG-72 antigen (58)	K_{eq} ($\times 10^9\ M^{-1}$) B72.3 2.5 CC92 14.3 CC49 16.2 CC83 27.1		(51)
G7A5 IgG and its fragments/A375 tumor cells	competitive binding assay	K_{eq}($\times 10^9\ M^{-1}$)	Sites/cell	(50)
		IgG 12	1.5×10^5	
		$F(ab')_2$ 12	1.2×10^5	
		Fab' 2.1	3.4×10^5	
IgG anti carcinoembryonic (CEA) antibodies/purified CEA	solid phase enzyme linked immunoadsorbent assay (59, 60)	K_{eq}($\times 10^9\ M^{-1}$) T84.66 47 ZCE025 6.8 T84.12 5.7		(61)
IgG murine T84.66 and its human chimeric form/purified CEA	(59, 60)	K_{eq}($\times 10^9\ M^{-1}$) T84.66 26 Chimeric 50		(62)
IgG 36-7-5/histocompatability antigen H-2K^k	cell binding assay (48)	$K_{eq} = 5 \times 10^8\ M^{-1}$ 2.9×10^4 sites/cell		(63)
IgG anti Lyb8.2 and its fragments/B cells	cell binding assay (48)	K_{eq}($\times 10^9\ M^{-1}$)	Sites/cell	(9)
		IgG 0.78	8×10^4	
		F(ab')2 0.7	4.5×10^4	
		Fab' 0.2	7.7×10^4	
IgG anti CEA antibodies/purified CEA	precipitation reaction (64)	K_{eq}'s ranging from 1×10^8 to $1.4 \times 10^9\ M^{-1}$		(65)
IgG 96.5/melanoma cells	uptake and washout of radiolabeled antibodies from tumor spheroids	$k_f = 2 \times 10^{-3}\ s^{-1}$ $Ag_o = 3 \times 10^{-8}$ M		

Notation used: K_{eq} = equilibrium binding constant, k_f = irreversible forward binding rate, Ag_o = molar concentration of binding sites.

measurement technique capable of quantifying mass transport and reaction parameters which accurately describe the physical situation of diffusion and immobilization of therapeutic agents in the interstitial space. Fluorescence recovery after photobleaching (FRAP) offers such ability. Total internal reflection microscopy (TIRM) alone or combined with FRAP has been used to quantify diffusion coefficients and equilibrium binding constants for interactions occurring on glass, plastic, and cell membrane surfaces. The theoretical model of FRAP with binding was proposed by Elson and Reidler (19) and expanded by Koppel (20) and Thompson et al. (21). TIRM has been used alone to investigate the kinetics of anti-DNP antibody with immobilized DNP at a surface (22). This is possible when the bound complex has measurably different optical properties than the individual species. TIRM with FRAP has been used to investigate the adsorption of BSA on fused silica surfaces (23) and on PMMA and PDMS surfaces (24) as well as the residence time of epidermal growth factor on erythrocyte ghost membranes (25). TIRM and fluorescence correlation spectroscopy (FCS) have also been used to investigate the binding at surfaces (26–30). Works by Elson (31, 32) and Petersen et al. (33) review the use of FRAP and FCS to measure kinetic parameters for interactions occurring at surfaces. Whereas TIRM techniques have been quite successful in studying two-dimensional binding on cell surfaces, they are not designed to quantify interactions occurring in a tissue mass (i.e., in bulk solution). Our laboratory has previously reported the development of a photobleaching technique capable of in vivo quantification of mass transport parameters. The technique's ability to quantify diffusion coefficients and convective velocities of serum soluble proteins has been validated in vitro (34) and demonstrated in normal and tumor tissue experiments in vivo (35). Recently, we have extended the principles and analysis established in the TIRM/FRAP literature to investigate the diffusion limited binding interaction of Concanavalin A with immobilized mannose (18). In this work we further refine the measurement technique, combining the benefits of video image digitization with

conventional photomultiplier data acquisition in an investigation of the reaction limited interaction of the monoclonal antibody B72.3 with the tumor associated antigen TAG-72. It is demonstrated that the reaction limited model should correctly represent most in vivo antibody/tumor associated antigen interactions. We report the equilibrium binding constant and concentration of binding sites for this system and discuss the potential in vivo use of this measurement technique.

GLOSSARY

Ab_{inc}	Incubating concentration of antibody (Molar M)
Ag	Concentration of vacant binding sites (M)
Ag_o	Total concentration of binding sites (M)
a	Radius of antigen bead (μm)
B-B72.3	BODIPY labeled B72.3 antibody
C_{ni}	Concentration of a given component (n = 1 unbound, n = 2 bound; i = a fluorescently active, i = b bleached) (M)
C_{Ta}	Total concentration of fluorescently active species (M)
C_{TB}	Concentration of fluorescently active species at the center of the bleach (M)
C_{TU}	Concentration of fluorescently active species far away from the bleach (M)
D	Diffusion coefficient (cm^2/s)
Da	Damkoehler number
erf	The error function
g	Acceleration of gravity (m/s^2)
I_{ni}	Fluorescence intensity of a given component (n = 1 unbound, n = 2 bound; i = a fluorescently active; i = b bleached) (Gray Levels GL)
I_{Ta}	Total fluorescence intensity (GL)
I_{TB}	Total fluorescence intensity at the center of the bleach (GL)
I_{TU}	Total fluorescence intensity far away from the bleach (GL)
I_{Avg}	Average fluorescence intensity in a given area (GL)
k_1	Association binding constant ($M^{-1}s^{-1}$)
k_{-1}	Dissociation binding constant (s^{-1})
nr	Fraction of total antibody that is biologically nonreactive
R_o	Gaussian radius of the photobleach
t	Time (s)
U_o	Bead settling velocity (μm/hour)
u	Dimensionless active region half length
β	Pseudoequilibrium constant
ϵ	Linearity constant between concentration and fluorescent intensity (M/GL)
γ	Dimensionless depth of the bleach
ξ	Half length of active region
μ	Viscosity of water (kg/m s)
τ	Dimensionless time
θ_{ni}	Dimensionless concentration or intensity of a given component (n = 1 unbound, n = 2 bound; i = a fluorescently active, i = b bleached)
θ_{Ta}	Dimensionless total concentration or intensity
θ_{avg}	Dimensionless average concentration or intensity
ϕ_o	Immobile fraction of ligand
ϕ_c	Immobile fraction of biologically active ligand
$\Delta\rho$	Difference in densities between water and the antigen beads (kg/m^3)

MODEL DEVELOPMENT

The binding model used in this study is identical to that outlined by Kaufman and Jain (18). Briefly, the model consists of the simple bimolecular interaction between ligand and receptor as shown in Eq. 1. This model has proven effective in modeling a wide range of biological binding interactions (22, 27, 36, 37). The diffusion equation with reversible binding to one type of site assuming a uniform distribution of binding sites, biologically active bleached molecules, immobile bound complex, no convective field, and no metabolism of the ligand or bound complex is (the validity of these assumptions for both in vitro and in vivo experiments have been addressed in [18]):

$$C_{1i} + Ag \underset{k_{-1}}{\overset{k_1}{\rightleftarrows}} C_{2i} \quad (1)$$

$$\frac{\partial C_{1i}}{\partial t} = D\nabla^2 C_{1i} - k_1 C_{1i} Ag + k_{-1} C_{2i} \quad (2)$$

$$\frac{\partial C_{2i}}{\partial t} = k_1 C_{1i} Ag - k_{-1} C_{2i}. \quad (3)$$

These equations[1] must be written for both fluorescently active (i = a) and bleached (i = b) macromolecules because bleached molecules are assumed to be biologically active. Experimentally, it is fluorescence intensity and not concentration that is measured. If the measured fluorescence intensity is linear with the concentration of fluorescently active macromolecule and is forced to have a zero intercept by background subtraction, concentrations may be rewritten in terms of the measured fluorescence intensity: $C_{ni} = \epsilon I_{ni}$. Epsilon is the linearity constant between concentration and fluorescence intensity.

As discussed in (18), the geometry of the system is cylindrical with dependence only in the radial direction

[1] C_{1i} = concentration of mobile macromolecule
C_{2i} = concentration of immobile (bound) macromolecule
Ag = concentration of vacant binding sites
Ag_o = total concentration of binding sites

(r) so that:

$$\nabla^2 C = \frac{1}{r}\frac{\partial}{\partial r}\left(r\frac{\partial C}{\partial r}\right). \quad (4)$$

The initial conditions are imposed by the Gaussian intensity profile of the laser beam and by the assumption that the bound and unbound components are in equilibrium and are bleached to the same extent.[2] The boundary conditions are:

$$\frac{\partial C_{1i}}{\partial r} = \frac{\partial C_{2i}}{\partial r} = 0 \quad \text{at} \quad r = 0 \quad \text{and as} \quad r \to \infty. \quad (5)$$

The recovery equations are rearranged so that the dimensionless average intensity reaches a value of 1 as $t \to \infty$, for a completely mobile system. The mathematical model of binding yields four coupled, nonlinear, partial differential equations describing the recovery of each of the four components (mobile fluorescently active, mobile bleached, bound active, and bound bleached). The recovery equation for the mobile active component is shown below.[3] (The Laplacian operator in Eq. 6 is dimensionless due to the fact that the length scale has been normalized with respect to R_o (see reference 18).) The remaining three equations are similar in form. Note the four contributions to the fluorescence recovery: diffusion, binding to unsaturated sites, negation of the association reaction due to saturation, and the dissociation reaction.

$$\frac{\partial \theta_{1a}}{\partial t} = \underbrace{\frac{D}{R_o^2}\nabla^2\theta_{1a}}_{\text{Diffusion}} - \underbrace{k_1 Ag_o\theta_{1a}}_{\text{Free Association}}$$

$$+ \underbrace{k_1\epsilon(I_{TU} - I_{TB})\theta_{1a}(\theta_{2a} + \theta_{2b} + \gamma)}_{\text{Saturation}} + \underbrace{k_{-1}(\theta_{2a} + \gamma)}_{\text{Disocciation}}. \quad (6)$$

[2] $C_{Ta}(r, t = 0) = C_{TB} + (C_{TU} - C_{TB})\left[1 - \exp\left(\frac{-2r^2}{R_o^2}\right)\right]$

C_{Ti} = total concentration of macromolecule = $C_{1i} + C_{2i}$ (the fluorescence intensity $I_{Ta} = I_{1a} + I_{2a}$ is measured)

C_{TU} = total concentration of fluorescently active macromolecule well beyond the bleached region

C_{TB} = total concentration of fluorescently active macromolecules at $r = 0$ and $t = 0$

R_o = radius of the bleached spot at $t = 0$ such that $C_T(R_o, t = 0) = (1 - 1/e^2)C_{TU}$, i.e., the Gaussian radius of the bleach

[3] γ is the dimensionless depth of the bleach defined as: $\gamma = C_{TB}/(C_{TU} - C_{TB})$

θ_{1a} = dimensionless intensity of mobile, fluorescently active macromolecule = $I_{1a}/(I_{TU} - I_{TB})$

θ_{2a} = dimensionless intensity of bound, fluorescently active macromolecules = $(I_{2a} - I_{TB})/(I_{TU} - I_{TB})$

θ_{2b} = dimensionless intensity of bound, bleached macromolecule = $I_{2b}/(I_{TU} - I_{TB})$

LIMITING CASES—ANALYTICAL SOLUTIONS

Analytical solutions to the above mathematical model have been derived for the three cases of (a) no binding, (b) diffusion limited binding, and (c) reaction limited binding. When no binding occurs, the simplified partial differential equations are easily solved using Fourier Transforms to yield the dimensionless fluorescence intensity as a function of space and time (35). This equation may be spatially integrated (18) to yield the dimensionless average fluorescence intensity (θ_{Avg}) in a square region of length 2ξ centered about the bleach as a function of time:

$$\theta_{Avg} = \frac{I_{Avg} - I_{TB}}{I_{TU} - I_{TB}} = 1 - \frac{\pi}{4u^2}erf^2\left(\frac{u}{\sqrt{1 + 8\tau}}\right), \quad (7)$$

where

$$u = \frac{\sqrt{2}\xi}{R_o} \quad \text{and} \quad \tau = \frac{Dt}{R_o^2}.$$

It is the quantity I_{Avg} that is measured during the photobleaching recovery.

When the system is diffusion limited (Damkoehler Number = $Da = (k_1 Ag_o R_o^2/D) \gg 1$ and system far from saturation) the bound and unbound components are rapidly exchanged and exist in equilibrium. Crank (38) demonstrates that such systems may be represented by the same solutions as for nonbinding regimes if the diffusion coefficient is replaced by an effective diffusion coefficient: $D_{eff} = D/1 + \beta$ where $\beta = k_1 Ag_o/k_{-1}$. Thus, diffusion limited binding systems are expected to have an asymptotic recovery to a value of $\theta_{Avg} = 1$ and are characterized by a single parameter, the effective diffusion coefficient. By measuring the effective diffusion coefficient and the diffusion coefficient of a nonbinding system, the product of the equilibrium constant and concentration of binding sites may be obtained (18). It has been shown (5) that β is the kinetic parameter of interest in predicting in vivo antibody distribution on macroscopic length and long time scales.

When the system is reaction limited ($Da \ll 1$) a given molecule exists in either the bound or unbound state with negligible exchange on the time scale of the fluorescence recovery. In this case, a fraction ϕ_o of the total molecules are effectively immobile on the time scale of the experiment. The dimensionless average fluorescence intensity θ_{Avg} for such a system will asymptotically approach a value less than unity due to the immobilized fraction which is not able to recover. In such a system, the kinetic parameters in the transient

equations may be neglected for short time scales and an analytical solution obtained. θ_{Avg} for a reaction limited system will be equal to:

θ_{Avg} = (fraction mobile)
× (recovery equation for mobile molecules)
+ (fraction immobile)
× (dimensionless average intensity at $t = 0$)

or:

$$\theta_{Avg} = \frac{I_{Avg} - I_{TB}}{I_{TU} - I_{TB}} = 1 - \frac{\pi}{4u^2}\left\{(1 - \phi_o)erf^2\left(\frac{u}{\sqrt{1 + 8\tau}}\right) + \phi_o \mathrm{erf}^2 u\right\} \quad (8)$$

The reaction limited system is thus characterized by two parameters, ϕ_o and D.

It is well known (12, 39, 40) that in the production, purification, labeling and storage of monoclonal antibodies, a given fraction of the labeled antibody will be rendered biologically inactive and will not be able to bind to its antigenic site. If nonreactive fraction data is available, it is appropriate to report the immobile fraction as the fraction of biologically active molecules which are immobile (ϕ_c) rather than merely ϕ_o. If nr is the fraction of antibody rendered biologically inactive then:

$$\frac{\phi_o}{1 - nr}. \quad (9)$$

The immobile fraction ϕ_c is a function of the equilibrium constant for immobilization (K_{eq}), the total concentration of binding sites (Ag_o), and the concentration of biologically active antibody (Ab_{inc}) in the system. By definition:

$$K_{eq} = \frac{C_{2a} + C_{2b}}{(Ab_{inc} - C_{2a} - C_{2b})(Ag_o - C_{2a} - C_{2b})} \quad (10)$$

upon rearrangement:

$$\phi_c = \frac{C_{2a} + C_{2b}}{Ab_{inc}} = \frac{\dfrac{1 + K_{eq}(Ag_o + Ab_{inc})}{K_{eq}Ab_{inc}} - \left(\left(\dfrac{1 + K_{eq}(Ag_o + Ab_{inc})}{K_{eq}Ab_{inc}}\right)^2 - \dfrac{4Ag_o}{Ab_{inc}}\right)^{0.5}}{2}. \quad (11)$$

The equilibrium binding constant and concentration of binding sites can thus be obtained by measuring ϕ_c as a function of incubating antibody concentration. In in vitro experiments, these parameters may also be obtained by measuring ϕ_c at various dilutions of the antigen.

SAMPLES

IgG (molecular weight 150,000) monoclonal antibody B72.3 (41) was the gift of Dr. B. Rhodes (RhoMed Inc., Albuquerque, NM).[4] The antibody was custom labeled with Boro Dipyro Methane Difluoride (BODIPY) fluorescent probe (Molecular Probes, Inc., Eugene, OR) to a dye to protein ratio of 2.93 and an antibody concentration of 0.42 mg/ml (2.8×10^{-6} M). Bovine Serum Albumin (1%) and Sodium Azide (2 mM) were added to the stock antibody to aid protein stability and inhibit bacterial growth. Antibody was stored at −72°C. Once thawed or incubated with antigen beads, samples were stored at 5°C. To measure the free diffusion coefficient of BODIPY B72.3, the stock solution of labeled antibody was drawn into a 200 μm thick glass capillary slide (model #W3520; Vitro Dynamics, Rockaway, NJ) for observation conducted at 23 ± 2°C. For B72.3 binding experiments, tumor homogenate containing tumor associated or irrelevant antigen immobilized to 5 μm diameter beads (RhoCheck Lot #J032990L1) donated by RhoMed Inc. was utilized as the immobilized antigen component. The beads were supplied as a 2% by volume solution of beads in PBS and 1% BSA. In binding experiments, an appropriate mixture of specific or control (irrelevant antigen) beads and a wash solution (PBS and 1% BSA supplied as part of the RhoCheck product) totaling 1.0 ml was centrifuged in order to concentrate the antigen beads. By altering the bead/wash solution mixture, various final bead concentrations were obtained. After centrifugation, 940 μl of the supernatant was removed and 50 μl of stock B72.3 antibody was then added. Samples were incubated at 5°C for at least 12 h before experimentation. As in the free diffusion experiments, samples were drawn into 200 μm thick capillary slides for observation at 23 ± 2°C. The capillary slide was inverted after each bleach (every 10 min) to avoid settling of the beads which would occur if the slide was left undisturbed for an hour or more. This experimentally observed settling time is in agreement with esti-

[4]B72.3 is an IgG1 (51). The antibody provided was purified from ascities fluid and aggregates were removed (personal communication, Dr. B. A. Rhodes, RhoMed Inc.). Free dye was removed during the custom labeling process (personal communication Dr. Rosaria Haugland, Molecular Probes Inc.), but was not assayed before photobleaching. The presence of free dye would be evidenced in a biphasic fluorescence recovery which was not seen experimentally.

mates assuming Stokes flow at infinite dilution.[5] Using this protocol, samples containing 18, 13.5, 9, and 4.5% by volume beads in 1.3×10^{-6} M antibody were obtained. In some experiments, the incubating antibody concentration was decreased in order to obtain larger immobile fractions.

EQUIPMENT FOR FRAP

The equipment, experimental procedure, and data analysis technique used in this study are those used and proposed by Kaufman and Jain (18). Briefly, the capillary slide was transilluminated for monitoring purposes at 480 nm by a mercury vapor lamp (Model HBO 100W; Zeiss, Morgan Instruments, Cincinnati, OH). Light passed through a heat reflector (Model Califax; Zeiss, Morgan Instruments), heat absorber (Model KG-1; Zeiss, Morgan Instruments), FITC exciter and red absorber filters (Models 46-79-79 and 46-78-85; Zeiss, Morgan Instruments). The microscope was focused on the sample using a 20X objective (Model F-LD 20/0.25; 46-06-05; Zeiss, Morgan Instruments). Light emitted from the sample was passed through a barrier filter (Model 46-78-33; Zeiss, Morgan Instruments) and the 1.25X lens in a Zeiss Optovar (Model 47-16-45; Zeiss, Morgan Instruments) installed in the microscope barrel. The image was monitored using an intensified charge coupled device (ICCD) camera (Model C2400-97; Hamamatsu, Photonic Microscopy Inc., Oak Brook, IL) operated in a range where measured intensity was linear with fluorophore concentration. The video signal was sent to an image analysis system (Model DT-IRIS; Data Translation, Marlboro, MA) housed in an IBM PC-AT allowing on-line digital analysis of the image.

A 5 W argon ion laser (488 nm) (Model 2000-5; Spectra Physics, Mountain View, CA) was used to photobleach the sample. The laser beam was directed through a spatial filter (Model 900; Newport Corp., Fountain Valley, CA) containing a 10X objective (Model M-10X; Newport Corp.) and a 25 μm pinhole aperture (Model 900PH-25; Newport Corp.). The beam was then focused using a 5X microscope objective (Model M-5X; Newport Corp.) and accessed the sample via the epiillumination port of the microscope where it was attenuated using neutral density filters (Models 46-78-40, -41, -42, Zeiss, Morgan Instruments). Two shutters (Uniblitz Electronic, Vincent Assoc., Rochester, NY) electronically controlled via the IBM PC-AT were used to control the bleaching time and light reaching the camera. The laser power was typically 0.36 mW after its passage through the spatial filter and objective. The 12% neutral density filter reduced the power impinging upon the sample to 0.04 mW whereas the 50% neutral density filter reduced the power to 0.18 mW.

EXPERIMENTAL PROCEDURE

After prefluorescent and prebleach (background) image acquisition and storage, a region in the sample was photobleached for 0.08–0.18 s. Upon closing the laser shutter, the camera shutter was opened to allow imaging of the sample. Single video frames were acquired as rapidly as allowed by the acquisition board, requiring ~0.16 s for each frame. The fluorescence intensity data from the active region (Fig. 1) was stored in the system buffers. To correct for nonuniform camera response or possible bleaching of the sample due to excitation light during fluorescence recovery, data was also obtained from a "control region" (Fig. 1). The process of data acquisition was continued for 24 s after the photobleach. After acquisition, background image subtraction, and correction for possible photobleaching due to the excitation light source, the 90 × 70 intensity data from the first time point were low pass filtered and a minimum in fluorescence intensity found in order to estimate the location of the bleached spot relative to the 90 × 70 pixel field. The bleach location was used to select a 36 × 29

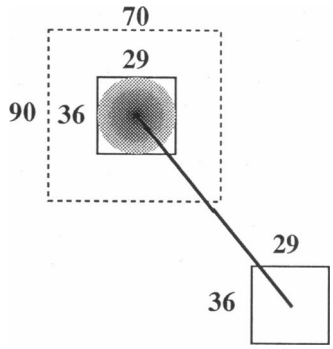

FIGURE 1 Data acquisition areas. The active region consisted of a 90 × 70 pixel (69 × 69 μm) area containing the bleached spot. Once the center point location of the bleach was estimated, data was collected from a 36 × 29 pixel (28 × 28 μm) active region properly centered about the bleach. A 28 × 28 μm control region was located along the vector passing through the active region and the center of the field of view and was placed so that it was an equal distance from the center of the field of view as the active region.

[5] $U_o = (2a^2\Delta\rho g/9\mu) = 59$ μm/h when $a = 2.5$ μm, $\Delta\rho = 1.21$ kg/m^3 (assuming the particles are glass), $g = 9.8$ m/s^2, and $\mu = 0.001$ (kg/m s). Smaller velocities would be calculated if the finite volume fraction of the antigen beads was taken into account.

pixel region properly centered about the photobleach (Fig. 1). The fluorescent intensity data in the 36 × 29 pixel region for the first time point as well as the average intensity in each 36 × 29 pixel region as a function of time were stored for subsequent analysis.

ANALYSIS PROCEDURE

Data analysis was performed on a Sun 3/260 workstation (Sun Microsystems Inc., Mountain View, CA). A Gaussian profile was fit to the intensity data as a function of position from the first time point using the Levenberg-Marquardt (42, 43) nonlinear parameter estimation method. This fit determined the parameters R_0 and I_{TB} which were used to convert the data into dimensionless form and to calculate the dimensionless active region size u. The diffusion coefficient and fraction of antibody which was immobile on the length scale of the recovery were obtained by using the Levenberg-Marquardt method to minimize the sum of squares error between the model (Eq. 8) and the dimensionless average fluorescence intensity in the active region as a function of time.

FLUOROMETRY

Fluorometry experiments were undertaken to independently verify the immobile fractions obtained in photobleaching experiments and to quantify the fraction of antibody which was biologically inactive. These experiments measured the fluorescence intensities of the antibody/bead mixtures before and after unbound antibody was washed from the samples in order to obtain the fraction of antibody bound to the antigen beads. The fluorescence intensity was measured using a luminescence spectrometer (Model LS-5B; Perkin Elmer, Norwalk, CT) with 490/520 nm excitation and emission wavelengths. A 45 μl cuvette (Model 105.251.QS; Hellma Cells Inc., Forest Hills, NY) contained the specimen. The zero level was first set using a solution of antigen beads containing no antibody at a volume percent equal to that of the sample to be tested. The fluorescence intensity of the antibody/bead sample was then measured. The sample was washed of free antibody by centrifuging the sample, discarding the supernatant and replacing it with an equal volume of wash solution. This process was repeated three times after which the fluorescence intensity attributed to the bound antibody was measured in the spectrofluorometer. The fluorescence intensity attributed to the bound antibody divided by the initial measurement of total fluorescence intensity in the sample represents the fraction of antibody bound to the antigen beads (ϕ). Photobleaching and fluorometry experiments used identical sample preparations. To obtain the fraction of antibody unable to bind, a sample containing 18% by volume TAG-72 beads in 1.3×10^{-8} M B-B72.3 antibody was used. It was assumed (see Discussion) that for a sufficiently large equilibrium binding constant and concentration of binding sites that nearly all of the biologically active macromolecule would be bound in this environment. Under this assumption, the immobile fraction measured represented the fraction of antibody biologically active.

TABLE 2 Results of photobleaching experiments

Sample	D ($\times 10^7$ cm^2/s)	ϕ_0	n
(1)	5.75 ± 0.72	0.04 ± 0.04	29
(2)	6.46 ± 1.06	0.11 ± 0.05	16
(3)	6.17 ± 1.17	0.31 ± 0.11	16
(4)	6.57 ± 1.05	0.26 ± 0.05	12
(5)	6.22 ± 1.30	0.16 ± 0.03	8
(6)	5.74 ± 1.14	0.12 ± 0.03	12
(7)	6.23 ± 1.60	0.34 ± 0.06	13

Values are reported as mean ± standard deviation, D = diffusion coefficient, ϕ_0 = uncorrected immobile fraction and n = number of bleaches. Sample identification is as follows: 1) 1.3×10^{-6} M BODIPY (B)-B72.3 2) 18% by volume control antigen beads in 1.3×10^{-6} M B-B72.3 3) 18% by volume specific antigen beads in 1.3×10^{-6} M B-B72.3 4) 13.5% by volume specific antigen beads in 1.3×10^{-6} M B-B72.3 5) 9% by volume specific antigen beads in 1.3×10^{-6} M B-B72.3 6) 4.5% by volume specific antigen beads in 1.3×10^{-6} M B-B72.3 7) 18% by volume specific antigen beads in 3.25×10^{-7} M B-B72.3.

RESULTS

The diffusion coefficients and immobile fractions obtained by photobleaching experiments are shown in Table 2. Representative Gaussian profiles and fluorescence recovery curves are shown in Fig. 2. The measured diffusion coefficient of the B72.3 antibody was independent of sample preparation[6] and measured immobile fraction (one way analysis of variance F statistic = 1.32 with $df_t = 6$ and $df_e = 99$. $p \sim 3.75$ at α level of 0.05). Small yet significant immobilization of the antibody on the glass surface was evidenced by an immobile fraction of four percent in the free antibody experiments. Significant immobilization was also noted in the irrelevant

[6]As discussed in reference 38, the diffusion coefficient should be a decreasing function of the volume fraction of beads. For a periodic distribution of spheres at 18% by volume, the diffusion coefficient is expected to be reduced by 25%. This was not seen in our data due to the fact that the length scale of the photobleach does not discern the bead distribution as a lattice.

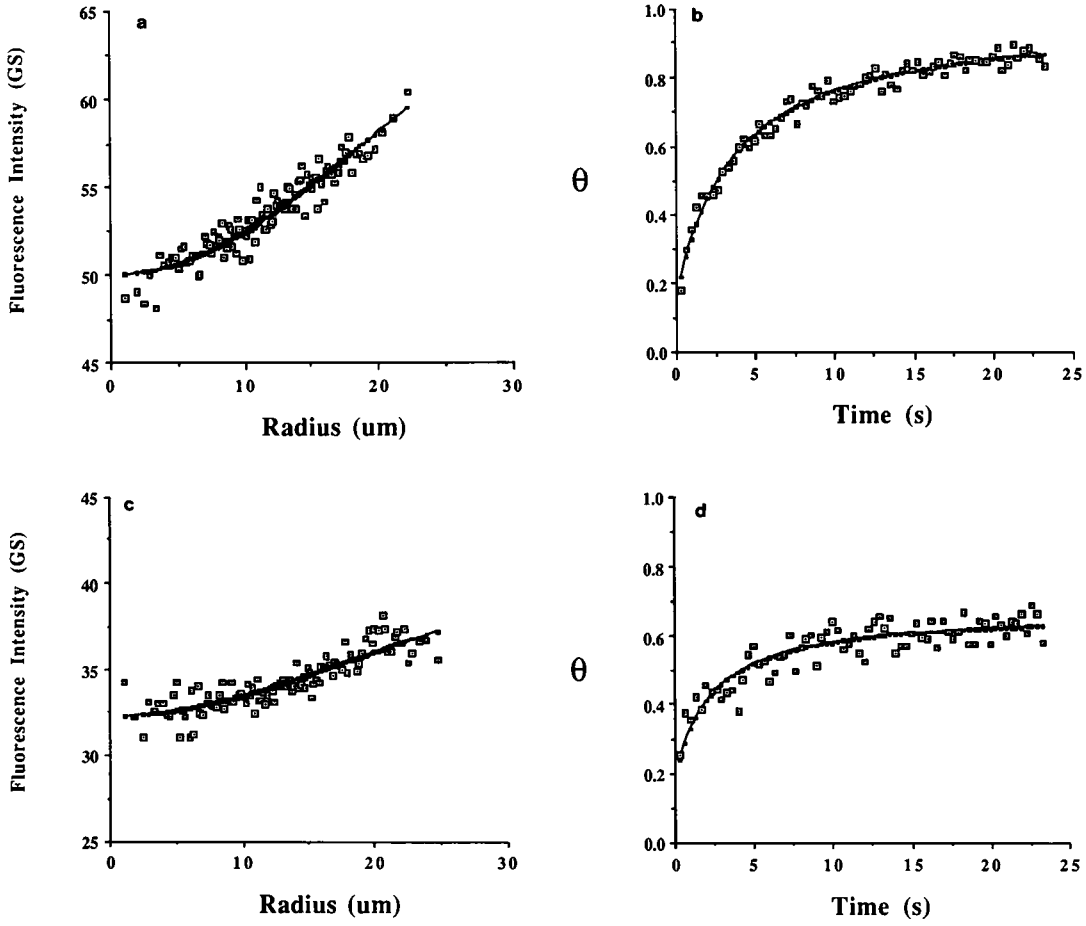

FIGURE 2 Photobleaching recovery. (*a* and *c*) Intensity data as a function of position for the first time point was fit to a Gaussian function in order to obtain the geometric parameters R_0 and I_{TB}. (*b* and *d*) Dimensionless average fluorescence intensity data as a function of time was fit to Eq. 8 to determine the diffusion coefficient and immobile fraction. *a* and *b* represent a photobleach of 2.8×10^{-6} M B-B72.3 which yielded $R_0 = 38.4 \pm 0.8$ μm, $I_{TB} = 50.0 \pm 0.1$ GS, $D = 6.08 \pm 0.28 \times 10^{-7}$ cm²/s and $\phi_0 = 0.03 \pm 0.01$. *c* and *d* are from a bleach of a solution containing 18% by volume antigen beads in 3.25×10^{-7} M B-B72.3. Measured parameters for this bleach were $R_0 = 35.1 \pm 1.7$ μm, $I_{TB} = 32.3 \pm 0.1$ GS, $D = 8.21 \pm 1.05 \times 10^{-7}$ cm²/s and $\phi_0 = 0.41 \pm 0.02$.

antigen sample. Immobile fractions measured by fluorometry were not statistically different from those obtained through photobleaching (student's *t*-test $p > 0.1$). In addition, fluorometry experiments demonstrated that 65% of the fluorescently active material was biologically inactive.

To quantify the equilibrium constant and concentration of binding sites for the interaction of biologically active B-B72.3 antibody with TAG-72 antigen beads, the 4% immobilization due to binding to the glass surface was subtracted from each ϕ_0 measurement, and ϕ_c calculated using Eq. 9 with $nr = 0.65$. The incubating antibody concentration was corrected to account for biologically inactive antibody. Photobleaching data of ϕ_c versus antigen dilution factor and incubating antibody concentration was fit to Eq. 11 using a nonlinear regression package (44) to yield the equilibrium binding constant and concentration of binding sites. Analysis of the covariance matrix indicated that these parameters operated independently with respect to predicting the data (44). An antigen dilution factor of 1.0 corresponded to a 18% by volume solution of antigen beads. Both antigen dilution factor and antibody concentration were independent parameters in fitting to Eq. 11 and all data were fit simultaneously. For purposes of display, ϕ_c versus antigen dilution factor at constant antibody concentration and ϕ_c versus incubating antibody concentration at constant antigen dilution factor are shown separately in Fig. 3. The photobleaching experiments yielded an antigen concentration of $4.4 \pm 0.6 \times 10^{-7}$ M for an 18% by volume solution of test beads and an equilibrium binding constant for the B-B72.3/TAG-72

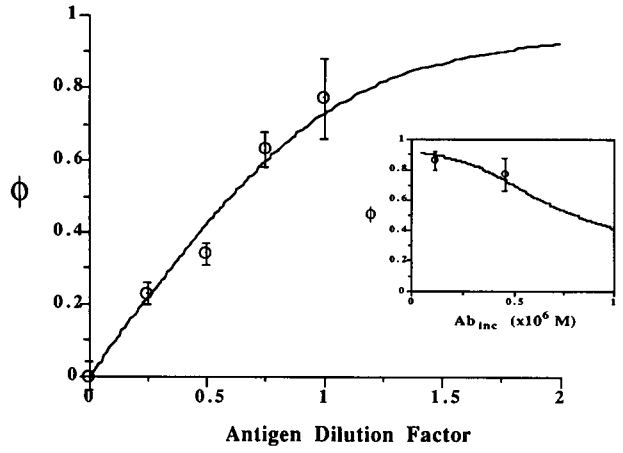

FIGURE 3 Fit to obtain K_{eq} and Ag_o. Nonreactive antibody corrected immobile fractions (ϕ_c) as a function of antigen dilution at constant incubating antibody concentration and as a function of incubating antibody concentration at constant antigen concentration were fit to Eq. 11 to obtain the equilibrium binding constant and antigen concentration for an 18% by volume solution of antigen beads. This procedure yielded $K_{eq} = 2.5 \pm 1.6 \times 10^7\ M^{-1}$ and $Ag_o = 4.4 \pm 0.6 \times 10^{-7}$ M. Error bars on the data represent the standard deviation of the measurement. "Antigen Dilution Factor" refers to the relative decrease in antigen concentration with respect to 18% by volume antigen beads. For example, a dilution factor of 0.5 represents a 9% by volume solution.

bead interaction of $2.5 \pm 1.6 \times 10^7\ M^{-1}$. Kinetic parameters obtained from fluorometry experiments were not statistically different (student's t-test $p > 0.1$). The average value of the diffusion coefficient for B-B72.3 antibody from all samples was $6.11 \pm 1.12 \times 10^{-7}\ cm^2/s$ ($n = 106$).

DISCUSSION

Independent measurement and possible FRAP experimental artifacts

Several factors were investigated to ensure that the immobile fraction obtained by photobleaching methods truly represented the fraction of fluorescently and biologically active antibody bound to the antigen beads. Immobile fractions were independently obtained through fluorometry experiments, and potential experimental artifacts were addressed. The immobile fractions obtained through fluorometry were in no case statistically different from those obtained in photobleaching experiments. Potential inaccuracy of fluorometry measurements due to antibody dissociation during the washing process of conversely, incomplete washing of the free antibody was not evidenced. Experimental artifacts could potentially cause error in the measurement of immobile fractions using FRAP. Bleaching of the specimen caused by the excitation (monitoring) light source during the process of fluorescence recovery would lead to an overestimation of the immobile fraction. The use of video image digitization enabled correction for this phenomena as data was acquired. In this study, the use of a control region placed apart from the photobleached spot, yet at an equal radius from the center of the field of view, corrected for factors influencing fluorescence intensity other than the fluorescence recovery process. To demonstrate that this control region correctly compensated for excitation bleaching, the algorithm was tested by its ability to report a constant fluorescence intensity in the active region as the sample was exposed to excitation light for a period of 100 s without prior bleaching from the laser. Fig. 4 demonstrates that the correction algorithm maintains constant fluorescence intensity readings and the possible error incurred by neglecting excitation bleaching. Previous studies have addressed potential protein cross-linking and laser induced photodamage (45, 46) and have discussed the implications of a limited domain or reservoir of fluores-

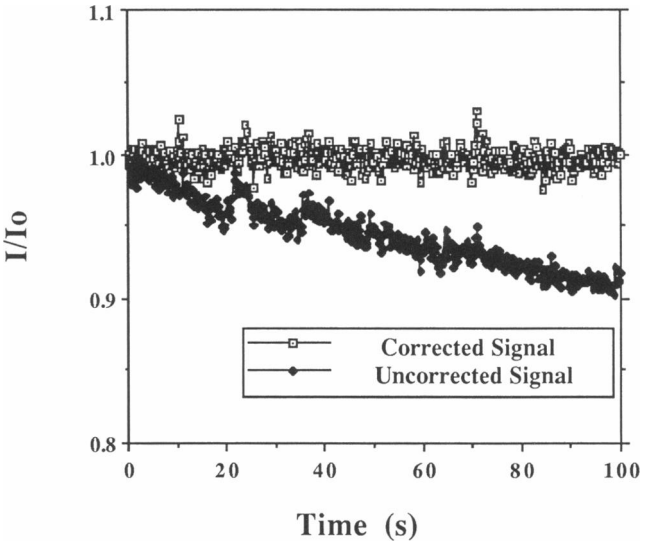

FIGURE 4 Test of control region correction algorithm. Sample containing 4.5% by volume antigen beads in 1.3×10^{-6} M BODIPY B-B72.3 antibody was excited with the same transillumination source as used in photobleaching experiments. Average fluorescence intensity data was acquired from an active region and control region located equidistant from the center of the field of view as the active region. The variation from the initial fluorescence intensity in the control region was calculated at each time point and the intensity in the active region corrected by this fractional change. Shown above is the corrected and uncorrected fluorescence intensity as a fraction of its initial value with time. Note that the correction algorithm maintains the intensity at its initial value, correcting for excitation bleaching and reducing random fluctuations.

cent macromolecule in the photobleached area (32). Both protein cross-linking and a limited domain would lead to an overestimation of the true immobile fraction of antibody. However, in our experiments, immobile fractions were not seen to increase with increased bleach exposure or repeated photobleaches at the same location.

Validity of reaction limited model

Errors in mass transport and reaction parameters can be incurred if the model of binding employed does not properly represent the interaction investigated. Goodness of fit alone can not be used as the sole criteria for determining the validity of a model, especially given the rather featureless shape of the fluorescence recovery curve. To investigate the validity of the reaction limited model, theoretical data were generated by numerical solution to the full set of partial differential equations describing fluorescence recovery (Eq. 6) and were fit to the reaction limited model (Eq. 8). The model's ability to correctly determine the diffusion coefficient and immobile fraction defined by the parameters used to generate the data established the range of validity of the reaction limited model. The reaction limited binding model assumes that diffusion is the dominant mode of fluorescence recovery on the time scale that the photobleach is monitored and that low frequency components of recovery due to binding interactions may be neglected without incurring error in measured diffusion coefficients or immobile fractions. Thus, the greater the magnitude of the diffusive component of fluorescence recovery, the greater the accuracy of the reaction limited model. The relative significance of the diffusive term has both spatial and temporal considerations. The magnitude of the diffusive term is a function of the Laplacian operator for the dimensionless concentration of mobile macromolecule. Due to the Gaussian initial condition, $\nabla^2\theta_{1a}$ decreased with distance from the bleach center. In addition, $\nabla^2\theta_{1a}$ also decreases with time as the gradient in fluorescence intensity relaxes, further lessening the contribution of the diffusive term and increasing the relative significance of the kinetic terms. Thus, the size of the active region and the monitoring time employed are important factors in determining the applicability of the reaction limited model. Simulations were conducted using parameter values representative of the photobleaching experimental conditions. The initial Gaussian radius of the bleach was set at 40 μm, the dimensionless active region size equal to 0.5, and the data generated for a period of 20 s.

In general, the reaction limited model correctly predicted the diffusion coefficient and immobile fraction for systems whose Damkoehler number was less than unity. These systems were characterized by a dominance of the diffusive term in the recovery equations (Fig. 5). For theoretically generated systems whose Damkoehler number was between 1 and 50, the model fit the recovery data well but yielded inaccurate parameters (Fig. 6). For larger *Da*, the reaction limited binding model was incapable of fitting the recovery data. Even when the Damkoehler number was less than unity, low extents of saturation caused slight error (~10%) in obtaining the diffusion coefficient due to the decreased significance of the diffusive term. When the reaction limited model was applied to theoretically generated nonreaction limited binding systems, the resulting diffusion coefficients and immobile fractions were seen to be functions of monitoring time due to the varying importance of the diffusive term (see caption of Fig. 6). This fact was used as a diagnostic to check the validity using the reaction limited model in the B72.3/TAG-72 binding system. Recovery curves for all of the experimental data were reanalyzed using only the data from the first 12 rather than 24 s. In no case were there significantly differences in the fitted parameters with decreased monitoring time (student's *t*-test $p > 0.05$), indicating that the experimental system

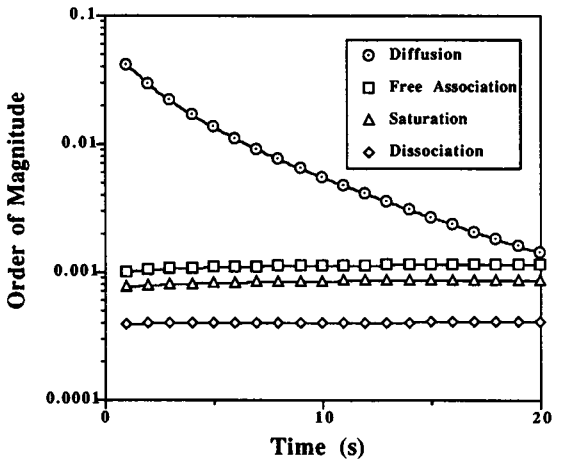

FIGURE 5 Order of magnitude of various kinetic contributions to fluorescence recovery at bleach periphery for a low Damkoehler number system. Theoretical simulation was conducted with the following parameter values: $D = 6.1 \times 10^{-7}$ cm²/s, $R_o = 4 \times 10^{-3}$ cm, $Ag_o = 4.4 \times 10^{-7}$ M, $u = 0.5$, $I_{TU} = 50$ GS, $I_{TB} = 37.5$ GS, $\epsilon = 9.1 \times 10^{-9}$ M · GS^{-1}, $k_1 = 2.5 \times 10^3$ M^{-1} · s^{-1} and $k_{-1} = 1 \times 10^{-4}$ s^{-1}. Order of magnitude of diffusion, free association, saturation and dissociation terms at the bleach periphery as a function of time were calculated numerically. The diffusive terms dominates the fluorescence recovery, especially at early time. The predominance of the diffusive term is even greater at locations toward the center of the bleach. Note also the log axis which visually understates the dominance of the diffusive term. In this simulation, $Da = 0.03$ and the reaction limited model correctly predicts a diffusion coefficient and immobile fraction of 6.1×10^{-7} cm²/s and 0.73, respectively, when the data is analyzed for 10 or 20 s.

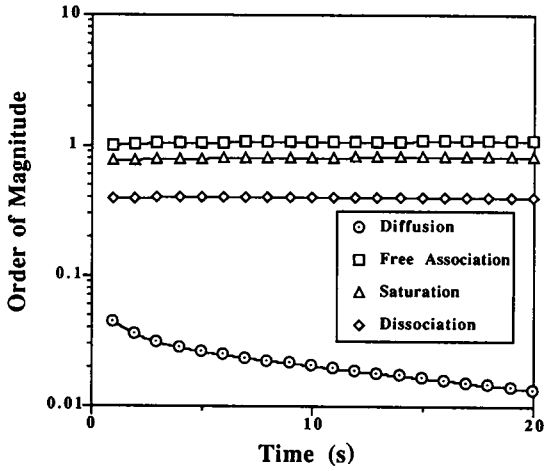

FIGURE 6 Order of magnitude of various kinetic contributions to fluorescence recovery at bleach periphery for a medium Damkoehler number system. Theoretical simulation was conducted with the following parameter values: $D = 6.1 \times 10^{-7}$ cm²/s, $R_o = 4 \times 10^{-3}$ cm, $Ag_o = 4.4 \times 10^{-7}$ M, $u = 0.5$, $I_{TU} = 50$ GS, $I_{TB} = 37.5$ GS, $\epsilon = 9.1 \times 10^{-9}$ M · GS^{-1}, $k_1 = 2.5 \times 10^6$ M^{-1} · s^{-1} and $k_{-1} = 1 \times 10^{-1}$ s^{-1}. Order of magnitude of diffusion, free association, saturation, and dissociation terms at the bleach periphery as a function of time were calculated numerically. The kinetic terms dominate the fluorescence recovery. In this simulation, $Da = 28.9$ and whereas the reaction limited model may fit the recovery data well, it yields incorrect parameters. When the reaction limited model is incorrectly applied, the parameters are seen to be functions of time. When the data were analyzed for 20 seconds, the reaction limited model gave a diffusion coefficient of 1.2×10^{-7} cm²/s and an immobile fraction of 0.05. When only the first 10 s of data were fit, the reaction limited model yielded $D = 1.8 \times 10^{-7}$ cm²/s and $\phi = 0.29$. Varying parameter values as a function of time may be used as a diagnostic for the proper use of the reaction limited model.

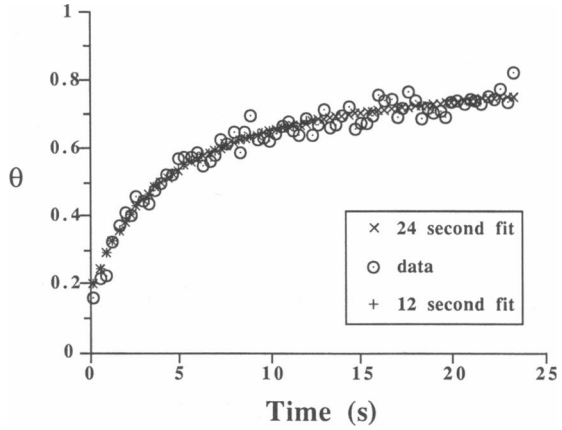

FIGURE 7 Diagnostic of reaction limited model with experimental data. When the reaction limited model is applied to nonreaction limited data, the mass transport and kinetic parameters obtained will be functions of monitoring time. Photobleaching data were reanalyzed using only the first 12 s of data rather than the full 24. There was no statistical difference between the parameters obtained from different monitoring times, confirming a reaction limited binding regime. Shown here is a fluorescence recovery curve (dimensionless average fluorescence intensity versus time) from a system composed of 13.5% by volume specific antigen beads in 1.3×10^{-6} M B-B72.3 antibody. The reaction limited model yields $D = 5.6 \times 10^{-7}$ cm²/s and $\phi_o = 0.18$ regardless of monitoring time.

was well characterized by the reaction limited binding model (Fig. 7).

Nonreactive fraction and free antigen

In any protein preparation, a fraction of the protein present will lack the biological reactivity under investigation. This is especially true in studies of labeled antibodies where purification, labeling, and storage, as well as the possible presence of labeled carrier protein such as BSA will lead to a fraction of the total fluorescent material being inactive in the sense of specific antibody reactivity. The magnitude of the nonreactive fraction must be accounted for to avoid error in estimating the concentration of binding sites and the antibody affinity (12, 39). In this study, if it were assumed that 100% of the fluorescently active material was capable of immobilization to the antigen beads, an equilibrium binding constant of $3.12 \pm 1.53 \times 10^5$ M^{-1} and a binding site concentration of $1.48 \pm 0.59 \times 10^{-6}$ M would have been obtained. In this study and in the commercial procedure for determining immunoreactivity (40) it is assumed that for low extent of saturation, all of the biological active antibody will be immobilized to the antigen beads. As can be demonstrated using Eq. 11, this assumption is not valid for small equilibrium binding constants. Significant error in estimating kinetic variables can occur if the nonreactive fraction is overestimated by attributing unbound antibody to a nonreactive fraction if it in fact is due to a small equilibrium constant for the receptor/ligand interaction. In this study, supernatants from the reactivity assay washes were assessed for biological activity. These supernatants lacked measurable reactivity to antigen specific beads, confirming the assumption that under the conditions of the reactivity experiment, all biologically active antibody was immobile and the reactivity assay was accurate.

Another possible confounding variable in these experiments is the possibility of antigen which has dissociated form the bead surface and is no longer immobile. This would lead to an overestimation of the nonreactive fraction and hence an overestimation of the kinetic parameters. The presence of free antigen would also tend to decrease the measured diffusion coefficient of the antibody due to the increased molecular weight of mobile antibody/antigen complexes. This phenomenon can easily be avoided by washing the antigen beads before antibody incubation but was not performed in

these experiments. We do not believe that appreciable free antigen was present in our binding samples however, due to the fact that the diffusion coefficient obtained in the absence of antigen beads was not significantly different than those obtained in binding samples.

Bivalent binding

The mathematical model of binding used in this study assumes that the equilibrium binding constant of the ligand/receptor interaction may be characterized by a single immobilization reaction. Because the B72.3 antibody is an IgG antibody, capable of bivalent antigenic binding, this assumption must be further investigated. It is seen that the occurrence of bivalent binding may be the major cause of discrepancies in equilibrium constants obtained by different laboratories, underscoring the need to characterize kinetics in the specific system of interest. The ability of an IgG antibody to bind bivalently at a surface will depend in a complex manner upon the antibody and receptor bulk concentration, the distance between binding sites on both the ligand and receptor, and the particular kinetic rate constants of the interaction (47). Bivalent binding will predominate when the density of vacant antigen on the surface is high, but will decrease with increasing degrees of saturation and increasing distances between neighboring antigenic sites on the surface. Obviously, the ability to bind bivalently will increase the overall effective equilibrium binding constant for immobilization of the ligand. Work by Dower et al. (48, 49) demonstrates an "enhancement factor" due to the presence of a mixture of bivalent and monovalent immobilization. Perelson et al. (47) and Pisarchick and Thompson (22) show that the effective equlibrium binding constant can be as high as the product of the two equilibrium constants for each immobilization step when bivalent binding is the predominant mechanism. This difference in affinity has been evidenced in differences in the effective equilibrium constants between an intact IgG molecule and its monovalent fragment (9, 48, 50) (see Table 1). If the equilibrium binding constant is $1 \times 10^7\ M^{-1}$ for a totally monovalent system, it is thus conceivable that the effective equilibrium constant in the presence of high antigen density and totally bivalent interaction could reach $1 \times 10^{14}\ M^{-1}$. The fact that the equilibrium binding constant reported here for the B72.3/TAG-72 binding systems is two orders of magnitude lower than that reported by Muraro et al. (51) is not surprising given the fact that Muraro's study used purified TAG-72 antigen immobilized at high density whereas this investigation utilized tumor homogenates immobilized to microscopic beads.

Potential in vivo use

The proposed photobleaching technique allows the quantification of bulk mass transport and reaction parameters in diffusion and reaction limited binding regimes. Unlike other techniques, it does not require measurable physical changes in the optical properties of the bound complex. Coupled with an appropriate animal model such as the rabbit ear chamber (52) or rat/mouse dorsal chamber tissue preparation (53), possessing an identified antibody/antigen interaction, this technique could be capable of in vivo quantification of mass transport and reaction parameters. Various assumptions of the proposed model as applied in vivo experimentation including neglecting convective flow, uniform distribution of binding sites, nonspecific binding, and thermal effects have been described previously (18). It is expected that in vivo, most antibody/antigen interactions will be well characterized by the reaction limited binding model. In vitro investigations have reported antigen densities on the order of 1×10^5 binding sites per cell (see Table 1). If the cellular volume fraction of the interstitial space is 50% and cells are assumed to have a diameter of 15 μm, this would translate into an antigen concentration of $\sim 5 \times 10^{-8}$ M. This small antigen concentration leads to small Damkoehler numbers and reaction limited binding regimes for most experimental conditions. It has been suggested by Koppel (20) that a reaction limited system could be rendered diffusion limited by increasing the length scale of the system (R_o for our purposes). This would be impractical in vivo where the length scale of the bleach is limited by the proximity of blood vessels which would contribute significant error were they to lay in the photobleached area.

At this point, it does not appear that individual rate constants may be determined from a single photobleach as we originally suggested (18). Components of fluorescence recovery due to association or dissociation are not discernable from that of diffusion in our current experimental protocol. This study obtained K_{eq} and Ag_o by measuring ϕ_c while varying both the antibody concentration and antigen dilution factor. In vivo these parameters would have to be obtained by slowly increasing antibody dosage and measuring ϕ as a function of antibody concentration in the interstitial space (54) as new steady states are reached after each bolus injection of antibody. As seen in reference 22 and demonstrated in this work, it is data at high values of ϕ_c that truly define the equilibrium binding constant. Theoretically, in Eq. 11 only two data points are needed to determine the two unknown parameters, yet realistically, several data points covering a wide range of ϕ_c values must be obtained for accurate determination of the equilibrium binding constant and concentration of binding sites. It

remains to be seen if this can be accomplished in vivo. Animal experiments to determine kinetic variables must possess an in vitro immobilization assay for the particular antibody/antigen system under investigation such as that discussed by Rhodes et al. (40) in order to report "true" kinetic constants. As discussed, the presence of nonreactive antibody will affect apparent antibody/antigen interaction. In cancer therapy, the presence of nonreactive antibody will also affect antibody uptake ratios in normal and tumor tissues (55).

This study, in combination with our previous work (18), has established the mathematical and experimental framework for the use of photobleaching to measure mass transport and reaction parameters in the bulk solution of the interstitial space in vivo. It is hoped that improved methods of cancer detection and treatment will result from the ability to accurately determine these parameters in the clinically realistic environment that this photobleaching technique affords.

The authors wish to thank R. Martin, C. Eskey, and Dr. F. Yaun for their valuable suggestions and assistance. In addition, we thank A. Lipton and Dr. M. Domach for their assistance in fluorometry experiments and Dr. B. Rhodes for donating the immunological reagents used in this study.

This work was supported by grants from the National Institutes of Health (CA-36902 and CA-49742), National Science Foundation (CBT-88-16062), and a Humboldt Senior Scientist Award to R. K. Jain. E. N. Kaufman is a recipient of a W. M. Keck Predoctoral Fellowship (1989–1990) and the Biomedical Engineering Society's Dr. Harold Lamport Award (1990).

REFERENCES

1. Covell, D. G., J. Barbet, O. D. Holton, C. D. Black, R. J. Parker, and J. N. Weinstein. 1986. Pharmacokinetics of monoclonal immunoglobulin G_1, $F(ab')_2$, and Fab' in Mice. *Cancer Res.* 46:3969–3978.
2. Weinstein, J. N., R. R. Egar, D. G. Covel, C. D. Black, J. Mulshine, J. A. Carrasquillo, S. M. Larson, and A. M. Keenan. 1986. The pharmacology of monoclonal antibodies. Ann. N.Y. Acad. Sci. 507:199–210.
3. Fujimori, K., D. G. Covell, J. E. Fletcher, and J. N. Weinstein. 1989. Modeling analysis of the global and microscopic distribution of immunoglobulin G, $F(ab')_2$, and Fab in tumors. *Cancer Res.* 49:5656–5663.
4. Thomas, G. D., M. J. Chappell, P. W. Dykes, D. B. Ramsden, K. R. Godfrey, J. R. M. Ellis, and A. R. Bradwell. 1989. Effect of dose, molecular size, affinity and protein binding on tumor uptake of antibody or ligand: a biomathematical model. *Cancer Res.* 49:3290–3296.
5. Baxter, L. T., and R. K. Jain. 1991. Transport of fluid and macromolecules in tumors III. Role of binding and metabolism. *Microvasc. Res.* 41:5–23.
6. Baxter, L. T., and R. K. Jain. 1991. Transport of fluid and macromolecules in tumors IV. A microscopic model of perivascular distribution. *Microvasc. Res.* 41:252–272.
7. Blasberg, R. G., H. Nakagawa, M. A. Bourdon, D. R. Groothuis, C. S. Patlak, and D. D. Bigner. 1987. Regional localization of a glioma-associated antigen defined by monoclonal antibody 81C6 in vivo: kinetics and implications for diagnosis and therapy. *Cancer Res.* 47:4432–4443.
8. Eger, R. R., D. G. Covell, J. A. Carraasquillo, P. G. Abrams, K. A. Foon, J. C. Reynolds, R. W. Schroff, A. C. Morgan, S. M. Larson, and J. W. Weinstein. 1987. Kinetic model for the biodistribution of an ^{111}in-labeled monoclonal antibody in humans. *Cancer Res.* 47:3328–3336.
9. Holton, O. D., C. D. Black, R. J. Parker, D. G. Covell, J. Barbet, S. M. Sieber, M. J. Talley, and J. N. Weinstein. 1987. Biodistribution of monoclonal IgG1, $F(ab')_2$, and Fab' in mice after intravenous injection: comparison between anti B cell (anti-LyB8.2) and irrelevant (MOPC-21) antibodies. *J. Immunol.* 139:3041–3049.
10. Sharkey, R. M., D. V. Gold, R. Aninpot, R. Vagg, C. Ballance, E. S. Newman, F. Ostella, H. J. Hansen, and D. M. Goldenberg. 1990. Comparison of tumor targetting in nude mice by murine monoclonal antibodies directed against different human colorectal cancer antigens. *Cancer Res.* 50:828s–834s.
11. Jain, R. K. 1989. Delivery of novel therapeutic agents in tumors: physiological barriers and strategies. *JNCI.* 81:570–576.
12. Lindmo, T., E. Boven, F. Cuttitta, J. Fedorko, and P. A. Bunn. 1984. Determination of the immunoreactive fraction of radiolabeled monoclonal antibodies by linear extrapolation to binding at infinite antigen excess. *J. Immunol. Meth.* 72:77–89.
13. McFadden, R., and C. S. Kwok. 1988. Mathematical model of simultaneous diffusion and binding of antitumor antibodies in multicellular human tumor spheroids. *Cancer Res.* 48:4032–4037.
14. Friedman, E., A. Thor, P. H. Hand, and J. Schlom. 1985. Surface expression of tumor-associated antigens in primary cultured human colonic epithelial cells from carcinomas, benign tumors, and normal tissues. *Cancer Res.* 45:5648–5655.
15. Hand, P. H., D. Colcher, D. Salomon, J. Ridge, P. Noguchi, and J. Schlom. 1985. Influence of spatial configuration of carcinoma cell populations on the expression of a tumor-associated glycoprotein. *Cancer Res.* 45:833–840.
16. Sutherland, R., F. Buchegger, M. Schreyer, A. Vacca, and J. P. Mach. 1987. Penetration and binding of radiolabeled anti-carcinoembryonic antigen monoclonal antibodies and their antigen binding fragements in human colon multicellular tumor spheroids. *Cancer Res.* 47:1627–1633.
17. Sung, C., R. J. Youle, and R. L. Dedrick. 1990. Pharmacokinetic analysis of immunotoxin uptake in solid tumors: role of plasma kinetics, capillary permeability and binding. *Cancer Res.* 50:7382–7392.
18. Kaufman, E. N., and R. K. Jain. 1990. Quantification of mass transport and binding parameters using fluorescence recovery after photobleaching: potential for in vivo applications. *Biophys. J.* 58:873–885.
19. Elson, E. L., and J. A. Reidler. 1979. Analysis of cell surface interactions by measurements of lateral mobility. *J. Supramol. Struct.* 12:481–489.
20. Koppel, D. E. 1981. Association dynamics and lateral transport in biological membranes. *J. Supramol. Struct.* 17:61–67.
21. Thompson, N. L., T. P. Burghardt, and D. Axelrod. 1981. Measuring surface dynamics of biomolecules by total internal reflection fluorescence with photobleaching recovery or correlation spectroscopy. *Biophys. J.* 33:435–454.

22. Pisarchick, M. L., and N. L. Thompson. 1990. Binding of a monoclonal antibody and its Fab fragment to supported phospholipid monolayers measured by total internal reflection microscopy. *Biophys. J.* 58:1235–1249.

23. Burghardt, T. P., and D. Axelrod. 1981. Total internal reflection/fluorescence photobleaching recovery study of serum albumin adsorption dynamics. *Biophys. J.* 33:455–468.

24. Tilton, R. D., C. R. Robertson, and A. P. Gast. 1990. Lateral diffusion of bovine serum albumin adsorbed at the solid-liquid interface. *J. Colloid Interface Sci.* 137:192–203.

25. Axelrod, D., R. M. Fulbright, and E. H. Hellen. 1986. Adsorption kinetics on biological membranes: measurement by total internal reflection fluorescence. *In* Applications of Fluorescence in the Biomedical Sciences. Alan R. Liss, Inc., New York. 461–476.

26. Thompson, N. L., and D. Axelrod. 1983. Immunoglobulin surface-binding kinetics studied by total internal reflection with fluorescence correlation spectroscopy. *Biophys. J.* 43:103–114.

27. Magde, D., E. Elson, and W. W. Webb. 1972. Thermodynamic fluctuations in a reacting system-measurement by fluorescence correlation spectroscopy. *Phys. Rev. Lett.* 29:705–708.

28. Magde, D., E. L. Elson, and W. W. Webb. 1974. Fluorescence correlation spectroscopy. II. An experimental realization. *Biopolymers.* 13:29–61.

29. Icenogle, R. D., and E. L. Elson. 1983. Fluorescence correlation spectroscopy and photobleaching recovery of multiple binding reactions I. Theory and FCS measurements. *Biopolymers.* 22: 1919–1948.

30. Icenogle, R. D., and E. L. Elson. 1983. Fluorescence correlation spectroscopy and photobleaching recovery of multiple binding reactions. II. FPR and FCS measurements at low and high DNA concentrations. *Biopolymers.* 22:1949–1966.

31. Elson, E. L. 1985. Fluorescence correlation spectroscopy and photobleaching recovery. *Annu. Rev. Phys. Chem.* 36:379–406.

32. Elson, E. L., and H. Qian. 1989. Interpretation of fluorescence correlation spectroscopy and photobleaching recovery in terms of molecular interactions. *In* fluorescence Microscopy of Living Cells in Culture Part B. Quantitative Fluorescence Microscopy-Imaging and Spectroscopy. D. Taylor and Y. Wang, editors. Academic Press Inc., New York. 307–332.

33. Petersen, N. O., S. Felder, and E. L. Elson. 1986. Measurement of lateral diffusion by fluorescence photobleaching recovery. *Handb. Exp. Immunol.* 1:24.1–24.23.

34. Jain, R. K., R. J. Stock, S. R. Chary, and M. Rueter. 1990. Convection and diffusion measurements using fluorescence recovery after photobleaching and video image analysis: In vitro calibration and assessment. *Microvasc. Res.* 39:77–93.

35. Chary, S. R., and R. K. Jain. 1989. Direct measurement of interstitial convection and diffusion of albumin in normal and neoplastic tissues by fluorescence photobleaching. *Proc. Natl. Acad. Sci. USA.* 86:5385–5389.

36. Kwok, C. S., and S. E. Cole. 1988. Uptake kinetics of monoclonal antibodies by human malignant melanoma multicell spheroids. *Cancer Res.* 48:1856–1863.

37. Gray, R. D., and R. H. Glew. 1973. The kinetics of carbohydrate binding to concanavalin A. *J. Biol. Chem.* 248:7547–7551.

38. Crank, J. 1975. The Mathematics of Diffusion. Clarendon Press, Oxford. 326–327.

39. Badger, C. C., K. A. Krohn, and I. D. Bernstein. 1987. In vitro measurement of avidity of radioiodinated antibodies. *Nucl. Med. Biol.* 14:605–610.

40. Rhodes, B. A., J. M. Buckelew, K. D. Pant, and G. H. Hinkle. 1990. Quality control test for immunoreactivity of labeled antibody. *BioTechniques.* 8:70–76.

41. Colcher, D., P. H. Hand, M. Nuti, and J. Schlom. 1981. A spectrum of monoclonal antibodies reactive with human mammary tumor cells. *Proc. Natl. Acad. Sci. USA.* 78:3199–3203.

42. Levenberg, K. 1944. A method for the solution of certain problems in least squares. *Quart. Appl. Math.* 2:164–168.

43. Marquardt, D. 1963. An algorithm for least squares estimation of nonlinear parameters. *SIAM J. Appl. Math.* 11:431–441.

44. Caracotsios, M. 1986. Model parametric sensitivity analysis and nonlinear parameter estimation. Theory and applications. Ph.D. Thesis., Department of Chemical Engineering, University of Wisconsin-Madison 1–279.

45. Sheetz, M. P., and D. E. Koppel. 1979. Membrane damage caused by irradiation of fluorescent concanavalin A. *Proc. Natl. Acad. Sci. USA.* 76:3314–3317.

46. Jacobson, K., Y. Hou, and J. Wojcieszyn. 1978. Evidence for lack of damage during photobleaching measurements of the lateral mobility of cell surface components. *Exp. Cell Res.* 116:179–189.

47. Perelson, A. S., B. Goldstein, and S. Rocklin. 1980. Optimal strategies in immunology III. The IgM-IgG switch. *J. Math. Biology.* 10:209–256.

48. Dower, S. K., K. Ozato, and D. M. Segal. 1984. The interaction of monoclonal antibodies with MHC class I antigens on mouse spleen cells I. Analysis of the mechanism of binding. *J. Immunol.* 132:751–758.

49. Dower, S. K., C. DeLisi, J. A. Titus, and D. M. Segal. 1981. Mechanism of binding of multivalent immune complexes to Fc receptors. 1. Equilibrium binding. *Biochemistry.* 20:6326–6334.

50. Le Doussal, J. M., A. Gruaz-Guyon, M. Martin, E. Gautherot, M. Delaage, and J. Barbet. 1990. Targeting of indium 111-labeled bivalent hapten to human melanoma mediated by bispecific monoclonal antibody conjugates: Imaging of tumors hosted in nude mice. *Cancer Res.* 50:3445–3452.

51. Muraro, R., M. Kuroki, D. Wunderlich, D. J. Poole, D. Colcher, A. Thor, J. W. Greiner, J. F. Simpson, A. Molinolo, P. Noguchi, and J. Schlom. 1988. Generation and characterization of B72.3 second generation monoclonal antibodies reactive with tumor-associated glycoprotein 72 antigen. *Cancer Res.* 48:4588–4596.

52. Sandison, J. C. 1924. A new method for microscopy study of living growing tissues by the introduction of a transparent chamber in the rabbit's ear. *Anat. Rec.* 28:281–287.

53. Algire, G. H. 1943. An adaptation of the transparent-chamber technique to the mouse. *J. Natl. Cancer Inst.* 4:1–11.

54. Armenante, P. M., D. Kim, and W. N. Durán. 1991. Experimental determination of the linear correlation between in vivo TV fluorescence intensity and vascular and tissue FITC-DX concentrations. *Microvasc. Res.* In press.

55. Yokoyama, K., C. H. Paik, J. C. Reynolds, V. K. Sood, S. M. Quadri, P. Maloney, C. Y. Min, S. Y. Shin, S. M. Larson, J. A. Carrasquillo, and R. C. Reba. 1987. Immunoreactivity affects the biodistribution and tumor targeting of radiolabeled anti-p97 Fab fragment. *J. Nucl. Med.* 28:651 abstract #392.

56. Wilson, B. S., E. Petrella, S. Lowe, K. Lien, D. G. Mackensen, D. S. Gridley, and D. R. Stickney. 1990. Radiolocalization of small cell lung cancer and antigen-positive normal tissues using monoclonal antibody LS2D617. *Cancer Res.* 50:3124–3130.

57. Ali, S. A., S. D. Warren, K. Y. Ritcher, C. C. Badger, J. F. Eary, O. W. Press, K. A. Krohn, I. D. Bernstein, and W. B. Nelp. 1990. Improving the tumor retention of radioiodinated antibody: Aryl carbohydrate adducts. *Cancer Res.* 50:783s–788s.

58. Heyman, B., G. Holmquist, P. Borwell, and U. Heyman. 1984. An enzyme linked immunosorbent assay for measuring anti-sheep erythrocyte antibodies. *J. Immunol. Methods.* 68:193–204.

59. Beatty, J. D., B. G. Beatty, and W. G. Vlahos. 1987. Measurement of monoclonal antibody affinity by non-competative enzyme immunoassay. *J. Immunol. Meth.* 100:173–179.

60. Beatty, J. D., B. G. Beatty, W. G. Vlahos, and L. R. Hill. 1987. Method of analysis of non-competitive enzyme immunoassays for antibody quantification. *J. Immunol. Meth.* 100:161–172.

61. Beatty, B. G., J. D. Beatty, L. E. Williams, R. J. Paxton, J. E. Shively, and M. O'Conner-Tressel. 1989. Effect of specific antibody pretreatment on liver uptake of ^{111}in-labeled anticarcinoembryonic antigen monoclonal antibody in nude mice bearing human colon cancer xenografts. *Cancer Res.* 49:1587–1594.

62. Neumaier, M., L. Shively, F. S. Chen, F. J. Gaida, C. Ilgen, R. J. Paxton, J. E. Shively, and A. D. Riggs. 1990. Cloning of the genes for T84.66, an antibody that has a high specificity and affinity for carcinoembryonic antigen, and expression of chimeric human/mouse T84.66 genes in myeloma and chinese hamster ovary cells. *Cancer Res.* 50:2128–2134.

63. Steller, M. A., R. J. Parker, D. G. Covell, O. D. Holton, A. M. Keenan, S. M. Seiber, and J. N. Weinstein. 1986. Optimization of monoclonal antibody delivery via the lymphatics: the dose dependance. *Cancer Res.* 46:1830–1834.

64. Kuroki, M., M. Kuroki, Y. Koga, and Y. Matsuoka. 1984. Monoclonal antibodies to carcinoembryonic antigen: A systematic analysis of antibody specificities by using related normal antigens and evidence for allotypic determinants on cacrinoembryonic antigen. *J. Immunol.* 133:2090–2097.

65. Kuroki, M., J. W. Greiner, J. F. Simpson, J. Primus, F. Guadagni, and J. Schlom. 1989. Serologic mapping and biological characterization of the carcinoembryonic antigen epitopes using fourteen distinct monoclonal antibodies. *Int. J. Cancer.* 44:208–218.